July 16, 2019 | vol. 116 | no. 29 | pp. 14389–14782

PNAS

Proceedings of the National Academy of Sciences of the United States of America www.pnas.org

Optimizing wind power production

Satellite record of Antarctic sea ice

Electronic polarization and photosystem yield

Facial expression in domestic dogs

Sensory brain activity and environmental constraints

Wind farm power optimization through wake steering

Michael F. Howland[a], Sanjiva K. Lele[a,b], and John O. Dabiri[a,c,1]

[a]Department of Mechanical Engineering, Stanford University, Stanford, CA 94305; [b]Department of Astronautics and Aeronautics, Stanford University, Stanford, CA 94305; and [c]Department of Civil and Environmental Engineering, Stanford University, Stanford, CA 94305

Edited by Alexis T. Bell, University of California, Berkeley, CA, and approved May 20, 2019 (received for review March 4, 2019)

Global power production increasingly relies on wind farms to supply low-carbon energy. The recent Intergovernmental Panel on Climate Change (IPCC) Special Report predicted that renewable energy production must leap from 20% of the global energy mix in 2018 to 67% by 2050 to keep global temperatures from rising 1.5 °C above preindustrial levels. This increase requires reliable, low-cost energy production. However, wind turbines are often placed in close proximity within wind farms due to land and transmission line constraints, which results in wind farm efficiency degradation of up to 40% for wind directions aligned with columns of turbines. To increase wind farm power production, we developed a wake steering control scheme. This approach maximizes the power of a wind farm through yaw misalignment that deflects wakes away from downstream turbines. Optimization was performed with site-specific analytic gradient ascent relying on historical operational data. The protocol was tested in an operational wind farm in Alberta, Canada, resulting in statistically significant ($P < 0.05$) power increases of 7–13% for wind speeds near the site average and wind directions which occur during less than 10% of nocturnal operation and 28–47% for low wind speeds in the same wind directions. Wake steering also decreased the variability in the power production of the wind farm by up to 72%. Although the resulting gains in annual energy production were insignificant at this farm, these statistically significant wake steering results demonstrate the potential to increase the efficiency and predictability of power production through the reduction of wake losses.

wind energy | turbulence | data science

The Intergovernmental Panel on Climate Change (IPCC) Special Report 15 on global warming (1) found that current rates of emissions will result in a temperature rise from preindustrial levels of 1.5 °C by 2040. Meanwhile, recent studies have predicted that the Paris Climate Agreement (2) will fail to keep warming below the stated goal of 2 °C (3, 4). The Special Report 15 found that coal-based electricity generation must decrease from contemporary rates of 40% of global energy production to 1–7%. As a result, renewable energy should compensate for this transition, increasing from 20% of energy generation in 2018 to 67% by 2050 (1). Wind and solar will likely comprise the bulk of these capacity additions due to their decreasing cost of electricity (5). While recent studies (5) have shown onshore wind energy to be economically favorable compared with coal and combined-cycle natural gas, such estimates are specific to sites with robust, reliable wind resource. To reach the goals of the Paris Climate Agreement, wind farms must significantly increase in number and density as well as extend to sites with less certain wind resource (6). As a result, methods to increase wind farm efficiency remain paramount to reducing carbon emissions.

While the major reason for decreased wind farm efficiency is variability in wind speed, aerodynamic losses within large arrays of turbines are also a key issue in wind farm operation (7). Due to the process of energy extraction from the atmospheric boundary layer, wind turbines necessarily produce a reduced momentum wake region immediately downstream (8). This wake will lower the power production of downstream turbines in the array. Wake power losses within a wind farm are a function of the incident wind speed and direction.

Wake losses occur when the wind speed is below the rated value (9) and turbines are at least partially aligned to the angle of the incoming wind. The mean wind speeds at the majority of wind farms are well below the rated value (10). Wind directions in the turbulent atmospheric boundary layer are inherently variable and will vary with the time of day, season, and other geophysical parameters (11). Wind farm layouts are designed to extract the maximum profit given historically observed wind direction and speed distributions, which typically results in larger streamwise turbine spacing in the most common wind directions. However, for other wind directions, wind turbines are more closely spaced (12). In worst-case scenarios of wind turbine spacing and inflow directions in contemporary wind farms, there is an over 40% loss of efficiency when the wind shifts to a direction aligned with the columns of the turbines (13).

To minimize the aerodynamic losses between turbines under prevailing wind conditions, the optimal streamwise spacing has been found to be $10–15D$, where D is the turbine diameter (14–16). Modern turbines are increasing in size, with offshore turbines now above 200 m in rotor diameter (17). The corresponding spacing of turbines multiple kilometers apart significantly increases the cost of transmission lines and land use (18). As a result, wind farm designers are left with a complex multiobjective optimization problem which typically results in operational turbine spacing of $6–10D$ (18). At this spacing, significant aerodynamic wake losses persist in modern wind farms when the flow is aligned with columns of turbines and the wind speed is below the rated value (13).

While the influence of wake losses on wind farm efficiency can be large for some inflow directions, the cumulative impact on the annual energy production of smaller wind farms is generally

Significance

Wake effects within wind farms can significantly decrease the power production and increase the cost of electricity. Herein, we designed a wake steering control scheme to increase the power production of wind farms. The wake steering method was tested in an array of six utility-scale turbines where it increased the power production for wind speeds near the site annual average between 7% and 13% and decreased variability by up to 72%, for selected wind directions at night. These improvements can contribute to the increasing ability of wind farms to provide reliable, low-cost, and efficient base energy load.

Author contributions: M.F.H. and J.O.D. designed research; M.F.H. performed research; M.F.H., S.K.L., and J.O.D. contributed new analytic tools; M.F.H., S.K.L., and J.O.D. analyzed data; and M.F.H., S.K.L., and J.O.D. wrote the paper.

The authors declare no conflict of interest.

This article is a PNAS Direct Submission.

Data deposition: The data from this paper have been deposited in the Stanford Digital Repository, https://purl.stanford.edu/rn821pp7681.

[1]To whom correspondence may be addressed. Email: jodabiri@stanford.edu.

This article contains supporting information online at www.pnas.org/lookup/suppl/doi:10.1073/pnas.1903680116/-/DCSupplemental.

Published online July 1, 2019.

lower since turbines are well spaced in directions of high wind speed. However, the impact of wake losses can be significant, as in the Horns Rev offshore wind farm where they have been found to reduce annual energy production on the order of 20% (13, 19). With wind farms increasing in size and quantity (20), wake losses are becoming an increasingly important factor in wind farm efficiency (21). While the magnitude of wake-induced efficiency degradation will depend on the specific wind farm site, methods which can reduce wake losses, once developed, will likely be broadly applicable to the global wind energy fleet. As such, potential wake mitigation methods have been a focus for multiyear research initiatives operated by the US Department of Energy such as the Atmosphere to Electrons (A2e) campaign and the Scaled Wind Farm Technology (SWiFT) facility (22). Given the broad potential impact of a method to mitigate wake losses, we have developed a control scheme and tested it on six utility-scale turbines in a wind farm in Alberta, Canada for wind speeds and directions where wake losses have been observed historically. Our method increased the power production for these wind directions between 7% and 13% for moderate wind speeds near the site annual average and up to 47% for low wind speeds, representing a statistically significant demonstration of wake steering power optimization for a multiturbine wind farm.

Aside from mean power production, wind turbine wakes contribute to intermittency. Intermittent power production is caused both by wind fluctuations in the turbulent atmospheric boundary layer and by the inherent nonlinearity of wind turbine power generation as a function of wind speed (23). Further, turbine wakes contribute to the lack of precise controllability of the wind farm power production. Intermittent renewable energy resources increase the need for costly energy reserve systems to guarantee grid service reliability (24). When wind speeds are low, wind turbines may oscillate about the cut-in speed as a result of wind gusts and dynamic wake meandering (25). Control methods which reduce the variability of the power production of wind farms, measured here as the SD of the time record of power generation, can decrease the ancillary service requirements for the energy grid (26). Our method, applied at the wind farm in Alberta, Canada, reduced the SD of the wind farm power production up to 72% for the wind conditions of interest.

Wake Steering Control

Recent attention has focused on mitigation of wake losses through the use of turbine control protocols and systems optimization that sacrifices individual turbine performance to improve the collective wind farm performance. Several studies have attempted to optimize the power generation of a wind farm through the operation of the upstream turbine in a suboptimal state to increase the efficiency of a downstream turbine (27, 28), but the results have not yet provided a conclusive solution that can be extrapolated to arbitrary wind farm configurations (29).

Contemporary turbine operation minimizes the yaw misalignment angle, which is the angle between the axis of the turbine nacelle and the incoming wind direction. While wind turbines typically exhibit small yaw misalignment due to control errors and sensor noise and uncertainty (30), the goal of industrial control algorithms is to minimize this yaw. When misaligned with respect to the incoming wind, wind turbines impose a lateral forcing which deflects the wake region (31), as sketched in Fig. 1*A*. While the misaligned turbine generates suboptimal power, the wake may no longer directly impinge upon a downstream turbine as a result of the wake steering. An application of wake steering for a six-turbine wind farm is shown in Fig. 1 *B* and *C*. Such a control strategy has been shown to be beneficial for downwind turbines in a number of wind tunnel experiments (32, 33) and computational studies (34–37). Wake

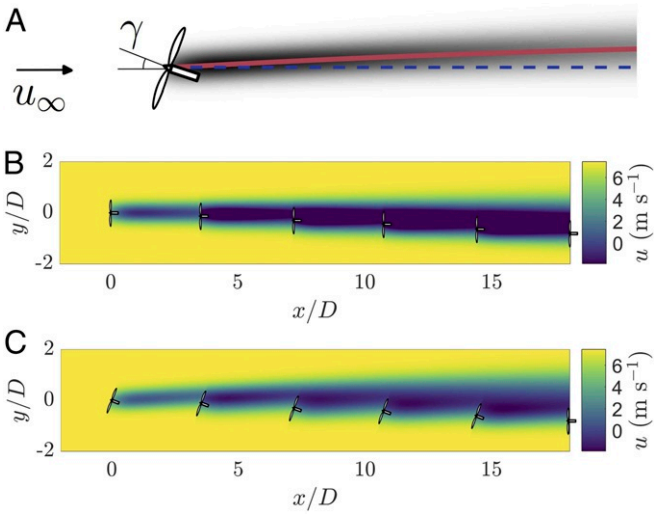

Fig. 1. (*A*) A wind turbine with diameter *D* yawed at angle γ with respect to the incoming wind and viewed from above. The incoming wind at speed u_∞ is incident from the left. The centerline of an unyawed, standard operational wake would follow the dashed blue line. The centerline of the yawed wake follows the solid red line. (*B* and *C*) Wake model streamwise velocity field for baseline maximum power point tracking control (*B*) and optimal yaw control (*C*). The incoming wind speed at the most upstream turbine is $u_\infty = 7.5$ m·s^{-1} and there are six turbines modeled. The wake following turbine six is not shown since the wake model automatically neglects calibration of the parameters for turbine six to increase computational efficiency.

steering has also been used in a two-turbine field experiment which demonstrated an increase in the downwind turbine power production as a function of the atmospheric stability (38). The impact of wake steering on the sum of the upwind and downwind turbines' power production was inconclusive in a separate two-turbine field experiment (39). Here we demonstrate a statistically significant effect of wake steering in a field study with a six-turbine unit.

Due to experimental difficulty and computational expense, parametric studies and real-time wind farm power optimization are limited with previous approaches (29). As such, the development of an accurate and computationally efficient model for wind farm power generation as a function of wake steering actuation is required to facilitate real-time closed-loop control (40).

Site-Specific Power Optimization

The wind turbine power, P, is a function of the wind farm layout and inflow conditions. Additionally, a wind turbine's power production is a function of its yaw misalignment angle as well as the yaw misalignment of upstream turbines which manifests as wake deflections. We have developed an analytic formulation to predict wind turbine power production as a function of atmospheric conditions and the yaw misalignment decisions of upwind turbines. Wake steering is captured using a recently developed lifting line model (41). While the magnitude of wake steering (42) and the wind speed and direction (43) are functions of the vertical dimension, the measurements available at the site in the present study were limited to pointwise sensors at hub height. While the incorporation of the curled-wake three dimensionality (42) may improve the model accuracy in certain atmospheric conditions, a 2D model is sufficient to capture the key physics for the present wind farm experiment. Details of the analytic predictive wake model are given in *SI Appendix*. The maximization of the wind farm power production through the use of wake steering is posed as an optimization,

$$\underset{\vec{\gamma}}{\text{maximize}} \quad \sum_{i=1}^{N_t} P_i$$
$$\text{subject to} \quad \gamma_i \in [\gamma_{min}, \gamma_{max}], \qquad [1]$$

where γ_i is the yaw angle for turbine i, N_t is the number of turbines, and γ_{min} and γ_{max} are bounds on the yaw misalignment for each turbine. Eq. **1** is not convex but can be optimized using a number of algorithms. Similar studies have previously used genetic algorithms (44) or discrete gradients (35). Since we have developed an analytic function to predict wind farm power production, Eq. **1** can be optimized efficiently using analytic gradients combined with the common gradient ascent strategy called Adam optimization (45).

Site-Specific Wake Model Calibration

The model (*SI Appendix*) is calibrated using utility-scale field historical data from five 1.8-MW Vestas V80 wind turbines and one 2.0-MW Vestas V80 turbine at an operational wind farm in Alberta, Canada. The six turbines in the wind farm are aligned at $\sim 335^\circ$, where north is 0° and the angle proceeds clockwise to 360° at north again. With wind inflow from 335°, the turbines are spaced by $\sim 3.5D$ in the prevailing wind direction. The wind inflow conditions are prescribed by the supervisory control and data acquisition (SCADA) nacelle-mounted measurements of wind speed and nacelle direction. Turbulence intensities were not measured in the present study due to the wind turbine hardware limitations. Details of the wind condition measurements are discussed in *SI Appendix*. Five years of 1-min averaged SCADA operational data, including power, nacelle direction, and wind speed, were used to calibrate the proportionality constant of the presumed Gaussian wake and the wake spreading coefficient. The latter parameter dictates the wake diameter which is a function of the streamwise distance following a wind turbine. This model allows each turbine to have independent values for the two model parameters, since these parameters are known to be a function of the atmospheric boundary layer conditions (46) as well as the number of upwind turbines (47). The model parameters were determined using analytic gradient descent (*SI Appendix*). The resulting calibrated model using the nocturnal historical baseline data is shown in Fig. 2 for $330^\circ \pm 5^\circ$ inflow at $u_\infty = 5{-}6$ m·s^{-1} and $u_\infty = 7{-}8$ m·s^{-1}. The power productions are normalized by the power of the most upwind turbine. The second turbine, on average, produces $\sim 30\%$ and 40% of the upstream turbine's power in the low and moderate wind speed cases, respectively. Wake losses are larger for lower wind speeds due to the higher relative thrust that the turbine imparts upon the velocity field at low wind speeds.

The model fit for the moderate wind speed has mean absolute error of 0.02 while the low wind speed fit has mean absolute error of 0.09 (given as a ratio normalized by the power of the first turbine). The less accurate fit in the low wind speed bin is expected due to the inherent nonlinearity at the effective cut-in velocity of 5 m·s^{-1} for the Vestas V80 turbines at the site of interest. Specifically, above cut-in, the turbine generates power and imparts drag on the fluid, creating a wake region. Below the cut-in, zero power is produced and no significant wake region exists. Due to dynamic wake meandering, downstream turbines will fluctuate between cut-in and shutdown for very low wind speeds and static models that consider only time-averaged behavior are not able to capture these dynamics as well (48). This is illustrated in Fig. 2*A* where zero power production occurs within 1 SD of the mean. Since the yaw controller on the Vestas V80 turbines did not allow for dynamic yaw maneuvers, such dynamic extensions were not applicable in the modeling framework. Wake model calibrations for other northwest wind inflow directions and speeds are not shown for brevity.

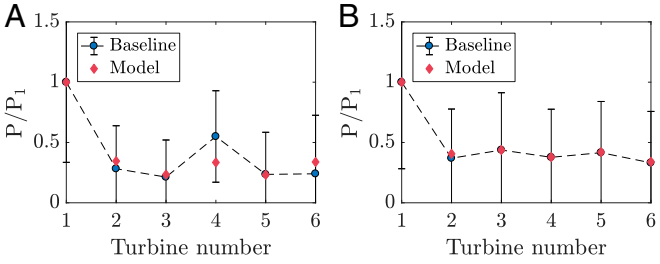

Fig. 2. (*A* and *B*) Wake model calibration using 5 y of historical SCADA turbine power data for inflow from $330^\circ \pm 5^\circ$ for (*A*) $u_\infty = 5{-}6$ m·s^{-1} and (*B*) $u_\infty = 7{-}8$ m·s^{-1}. Error bars represent 1 SD in the data. Turbine 4 is a Vestas V80 2.0-MW machine while the rest are Vestas V80 1.8 MW. The turbine power productions are normalized by the most upwind turbine P_1.

Field Experiment Design

While the wind farm in Alberta was designed for high-speed flow from the southwest, nocturnal low to moderate wind speeds from the northwest occur during the summer and fall. The present experiment aimed to optimize the yaw misalignment angles for these wind speeds from the northwest for which there are significant wake effects.

The yaw misalignment optimization was run with the calibrated model for inflow from 315° to 355° for which wake losses are observed. These angles represent $\sim 8\%$ of the nocturnal operation of the wind farm with nearly all of the samples occurring in the summer and fall seasons. The historical data wind rose is shown in *SI Appendix*, Fig. S1*A*. The yaw angle optimization resulted in $\sim 20^\circ$ clockwise yaw misalignment with respect to the incoming wind for each of the first five turbines in the column and zero misalignment for the turbine that was farthest downwind. Due to the hardware limitations of the yaw control systems of the wind turbines, only one set of yaw misalignment angles could be chosen for the range of northwest inflow. Therefore, the misaligned turbines were persistently offset by 20° for all northwest inflow directions, from 315° to 355°. While turbulence intensity measurements were not available at the wind farm site, the nocturnal operation typically results in fairly low turbulence intensity and therefore larger wake losses due to suppressed mixing in the wakes (11). Details of the yaw misalignment optimization are given in *SI Appendix*. Other yaw misalignment angles were not tested due to experimental limitations of implementation and to increase the number of unique days of experimentation with one set of misalignments. The longer experiment duration was necessary to achieve statistical confidence.

The present control-based optimization strategy was tested in a full-scale field experiment of the six utility-scale turbines from October 15 until October 25 of 2018. A photo of the yaw-misaligned turbines can be seen in Fig. 3*A*. A top-view sketch of the optimal yaw angles for reference inflow from the northwest can be seen in Fig. 3*B*.

Field Experiment Results

Significant power increases over the baseline were observed for low to moderate wind speeds from the northwest. The impact of the wake steering on the mean and SD of the power production for the northwest inflow conditions is shown in Table 1. Wind directions and speeds with more than 15 1-min–averaged data samples are shown.

For low wind speeds of $u_\infty = 5{-}6$ m·s^{-1} and $325^\circ \pm 5^\circ$ inflow, the total power of the six turbines increased from a temporal average of 390 kW to 570 kW, representing a 47% increase. Meanwhile, for $330^\circ \pm 5^\circ$ inflow at $u_\infty = 5{-}6$ m·s^{-1}, the power increase was 28% (Fig. 3*C*). The large percent increases in these cases are due to the low power production at low wind speeds and the proximity of the wind speeds to the cut-in speed of 5 m·s^{-1}.

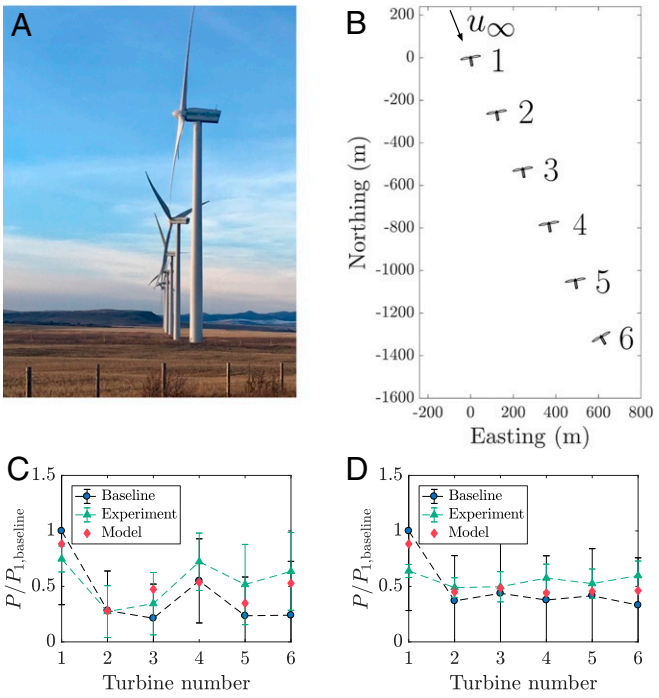

Fig. 3. (*A*) Photo of the six Vestas V80 turbines at the operational wind farm in Alberta, Canada. (*B*) Top view of the optimized yaw misalignment for the six turbines. The flow originates from the northwest, the inflow condition of interest for the present optimization experiment. Turbines one through five are misaligned 20° clockwise with respect to the incoming wind. Turbine six is not misaligned. Coordinates are in meters. (*C* and *D*) The power as a function of turbine number is compared for baseline operation with 5 y of historical SCADA data (blue circles), the experimental yaw campaign (green triangles), and the model predictions (red diamonds) based on the calibrations given in Fig. 2. The inflow conditions are shown for $330° \pm 5°$ at (*C*) $u_\infty = 5{-}6$ m·s^{-1} and (*D*) $u_\infty = 7{-}8$ m·s^{-1}. Error bars represent 1 SD in the data.

The significant improvement in these two cases can be attributed to the deflection of the upstream wakes. Partial wake overlap occurs when a section of the wind turbine rotor area is in the wake of an upwind turbine while another section is in unperturbed, freestream flow. Such a case occurs for the six turbines with flow from 325 ° to 330 °. During the partial wake scenario, a small yaw misalignment for the upwind turbine can result in the downstream turbine operating exclusively in freestream conditions. The reduction in the occurrence of partial waking is beneficial for power generation and significantly reduces turbine fatigue and failure (49). The model captures the influence of yaw misalignment in the partial wake scenario as shown in Fig. 1 *B* and *C*, where the wakes of the upstream turbines are deflected away from downstream turbines. The wakes impact the downstream turbines more directly at 330° than at 325°. As a result, larger wake deflections are required at 330° than at 325° to steer the wake away from the downstream turbines. Therefore, the anticipated power increase is higher for 325° where the partial wake scenario is most prominent.

For the higher wind speed of $u_\infty = 7{-}8$ m·s^{-1} from $330° \pm 5°$ the total power increased from 1.86 MW to 2.11 MW, a 13% increase (Fig. 3*D*). The percentage increase is less in the higher wind speed cases as a result of the decreased wake effects at these speeds.

Flow directly impinging along the alignment of the wind farm column at $335° \pm 5°$ occurred significantly only at wind speeds between $u_\infty = 7{-}8$ m·s^{-1}. For these conditions, the power production of the six turbines increased by 7%. Wind farms are typically sited at locations in which the mean wind speed is around 8 m·s^{-1} (10). Therefore, for wind farms with similar streamwise spacing and direct alignment, the 7% power increase observed in this wind condition is expected on average.

Wake steering also significantly reduced the variability in the sum of the six-turbine power production, measured here as a SD in the time series of 1-min–averaged data (Table 1). The reduction in the SDs of the sum of power is due to the diminished wake effects between the turbines. This manifests as a notable decrease in the percentage of time the turbines are not producing power (off rate) for all wind conditions. It is worth noting that all of the wind conditions considered here are above the cut-in speed of the Vestas V80 turbines and therefore without wake effects the off rate would be 0% for all wind condition cases. The high off rates in the baseline control case result from the impinging speed to a given turbine dropping below the cut-in speed. As a result of the wake steering, the percentage of time in which the speed decreases below the cut-in value for the downwind turbines has appreciably dropped.

The low-order model is able to predict the effect of the yawing action on the trends of power production in the field experiment based on calibration using only historical data (Fig. 3 *C* and *D*). As expected, the power production of turbine one (i.e., the most upwind turbine) was reduced due to operation with yaw misalignment. However, the power production of turbines two through five, and especially the farthest downwind turbine six, increased significantly. There are discrepancies in the low wind speed case shown in Fig. 3*C* as a result of the cut-in speed nonlinearity and dynamic wake meandering not captured in the model. However, the qualitative agreement with the model prediction trends promotes the use of the present model for real-time control of arbitrary, utility-scale wind farms.

The largest source of error in the present modeling framework is the functional dependence of power on the yaw misalignment angle. In the present approach, the power production as a function of yaw was assumed to follow the wind tunnel experimental result of $\cos^2(\gamma)$ (50). While this model works fairly

Table 1. Six utility-scale wind turbine wake steering effects on the mean (Δ_m), SD(Δ_s), and off rate of power production compared with the baseline operation

		Experimental results				
Wind inflow: Direction, °	Wind inflow: Speed, m·s^{-1}	Δ_m, %	Δ_s, %	Baseline off rate, %	Yawed off rate, %	No. of data points
320	5–6	−13	−53	31	24	65
325	5–6	+47	−20	36	13	52
325	6–7	+24	+2	24	12	25
330	5–6	+28	−14	27	10	17
330	7–8	+13	−72	18	0	22
335	7–8	+7	−73	12	0	22

Conditions of northwest inflow with more than 15 1-min–averaged samples are shown.

Table 2. Two-sample Kolmogorov–Smirnov statistical test for the null hypothesis that the baseline historical SCADA power data and the experimental yaw misalignment power data are samples of the same distribution

Wind inflow: Direction, °	Wind inflow: Speed, m·s^{-1}	*P* values		
		Full	10,000	100,000
320	5–6	0.13	0.14	0.14
325	5–6	$2.3 \cdot 10^{-7}$	$6.1 \cdot 10^{-4}$	$6.1 \cdot 10^{-4}$
325	6–7	0.043	0.32	0.32
330	5–6	0.039	0.27	0.27
330	7–8	$6.9 \cdot 10^{-6}$	0.015	0.015
335	7–8	$8.0 \cdot 10^{-5}$	0.03	0.03

The Kolmogorov–Smirnov test is run with the full historical dataset (full) and with Monte Carlo sampling from the full dataset such that the number of samples is consistent between the baseline and the experimental campaign. The Monte Carlo statistical method is run for 10,000 and 100,000 random samples to demonstrate convergence.

well in the low wind speed case shown in Fig. 3*C*, it is inaccurate for the higher wind speed case shown in Fig. 3*D*. As a result, there is likely a functional dependency of the exponent of cosine on the incoming wind speed as well as the previously reported dependence on the turbine type (44) and shear and veer in the atmospheric boundary layer.

The power increase results are statistically significant ($P < 0.05$) according to a two-sample Kolmogorov–Smirnov test. The details of the statistical experiments are shown in *Materials and Methods*. However, the statistical test does not examine the dominant causes of uncertainty, which are atmospheric boundary layer inflow conditions including wind speed and direction and the limited number of unique days of the experimental yaw campaign. The full dataset can be accessed at https://purl.stanford.edu/rn821pp7681.

Discussion

We demonstrate a statistically significant utility-scale field experiment of wake steering increasing the power production of a multiturbine wind farm for wind conditions which exhibit wake losses. While the impact of wake steering on annual energy production is site specific (e.g., below 0.3% at this wind farm), this experiment serves as a proof of concept for the potential of wake steering to significantly mitigate wake losses which reduce the annual energy production of wind farms (13). Wake steering control also decreased power production intermittency. Since frequency regulation ancillary services are required on the timescale of minutes (26), the SDs with respect to 1-min–averaged time series of power production are relevant to energy grid planning. This demonstrates that wake steering has the potential to reduce the intermittency of wind energy and thus improve the reliability of this component of the energy grid. Advances in our understanding of the physics of wind farms, combined with improvements in modeling, design, and control optimization, will further expand the value of this renewable energy technology and its ability to provide low-cost and reliable energy for a sustainable grid.

Achieving these potential power increases in the global wind farm fleet requires an efficient computational model. The present analytic model formulation was chosen due to its computational efficiency, which facilitates its use for real-time control of utility-scale wind farms. The computational cost of previous methods scales as $O(N_x N_y)$, where N_x and N_y are the number of grid points used in the computational domain, whereas the cost of the present method scales as $O(N_t)$, where N_t is the number of turbines. Typically, $O(10)$ grid points are used for each turbine in the wind farm (34), leading to an approximate scaling of $O(100N_t^2)$. Therefore, the present method has a computational reduction of at least two orders of magnitude. This scaling enables real-time model calibration and wind farm control using only a standard personal computer. Given that all utility-scale wind turbines are constructed with yaw controllers, the present control scheme can be directly implemented into any operational wind farm, thus immediately increasing the energy outputs from these sites with no additional cost.

Recent simulations have noted a potential influence of the direction of yaw misalignment on the power production in a simplified, aligned, two-wind-turbine wake steering scenario (51, 52). This observation has not been corroborated in all other wake steering studies and is likely a strong function of the turbine layout (53). The potential asymmetry in the power production as a function of the direction of yaw misalignment is likely caused by the curled, 3D wake (42) and the wind velocity veer and shear. Recent work suggests that this asymmetry is due to the Coriolis effect (37). These effects are the subject of ongoing modeling work (36, 43, 54, 55) and were therefore not included in the present framework.

Aside from the effect of yaw misalignment on power production observed here, wake steering will also have an impact on wind turbine unsteady loading and therefore mechanical fatigue. Theoretical and numerical studies have predicted that yaw misalignment can reduce or increase the mechanical fatigue loading on wind turbine blades, depending on the direction of yaw misalignment (56). However, the influence of yaw misalignment on fatigue loading is a function of the specific wind turbine and control system as recent studies have reported differing results, depending on the wind turbine of interest (49, 57). Further, yaw misalignment can reduce the occurrence of partial wake overlap which is known to significantly increase fatigue loading (58). In the experiment described here at a wind farm in Alberta, partial wake overlap decreased significantly. While the wind turbine fatigue loading was not measured in the present field experiment, it is the subject of future work and instrumentation at this field site. More generally, accurate predictions of the influence of yaw misalignment on the fatigue loading of all of the wind turbines in the wind farm will likely be required before the broad implementation of wake steering as the optimal control scheme for utility-scale wind farms. This is the subject of ongoing work through the Department of Energy A2e program through the use of the National Renewable Energy Laboratory's FAST simulation tool (59).

Materials and Methods

Statistical Tests. The statistical significance of the experimental yaw power optimization results was tested using the two-sample Kolmogorov–Smirnov test. The Kolmogorov–Smirnov test was selected since the datasets are non-normal distributions. The null hypothesis is that the sum of the six-turbine power generations from the baseline historical data and the experimental yaw measurements are the same distributions. The statistical test is run for the specific inflow conditions shown in Table 1. There are more than an order of magnitude more samples from the historical baseline dataset than for the yaw campaign due to the limited length of the field experiment. As such, the *P* values are computed using random sampling from the full distribution such that the baseline dataset has the same number of data points as the yaw misalignment experiment data. The *P* values are then averaged together as a Monte Carlo method. The resulting *P* values are shown in Table 2. All results are statistically significant ($P < 0.05$) except for inflow from $320° \pm 5°$ at a speed of 5–6 m·s^{-1}. The samples during the experimental yaw misalignment campaign are not strictly independent since they may occur during similar atmospheric boundary layer conditions. The results are similar if smaller wind speed or direction bins are used to calculate conditional averages. The full dataset can be accessed at https://purl.stanford.edu/rn821pp7681.

ACKNOWLEDGMENTS. We thank TransAlta Corporation and TransAlta Renewables for graciously providing historical wind farm operational data and for performing the yaw misalignment experimental campaign on operational turbines. M.F.H. is funded through a National Science Foundation Graduate Research Fellowship under Grant DGE-1656518 and a Stanford Graduate Fellowship.

1. Intergovernmental Panel on Climate Change. "Summary for policymakers" in *Global Warming of 1.5°C. An IPCC Special Report on the Impacts of Global Warming of 1.5°C Above Pre-Industrial Levels and Related Global Greenhouse Gas Emission Pathways, in the Context of Strengthening the Global Response to the Threat of Climate Change, Sustainable Development, and Efforts to Eradicate Poverty*, V. Masson-Delmotte *et al.*, Eds. (World Meteorological Organization, Geneva, Switzerland, 2018).
2. UNFCCC, "Adoption of the Paris agreement" (Report No. FCCC/CP/2015/L.9/Rev.1, 2015).
3. J. Rogelj *et al.*, Paris agreement climate proposals need a boost to keep warming well below 2 C. *Nature* **534**, 631–639 (2016).
4. K. Anderson, G. Peters, The trouble with negative emissions. *Science* **354**, 182–183 (2016).
5. EIA, "Annual Energy Outlook" (AEO2018, 2018).
6. C. L. Archer, M. Z. Jacobson, Evaluation of global wind power. *J. Geophys. Res. Atmos.* **110**, 110.D12 (2005).
7. R. Wiser, M. Bolinger, "2017 wind technologies market report" (Tech. Rep. DOE/EE-1798, US Department of Energy Office of Energy Efficiency and Renewable Energy, US Department of Energy Office of Scientific and Technical Information, Oak Ridge, TN, 2017).
8. L. Vermeer, J. N. Sørensen, A. Crespo, Wind turbine wake aerodynamics. *Prog. Aerospace Sci.* **39**, 467–510 (2003).
9. M. A. Abdullah, A. Yatim, C. W. Tan, R. Saidur, A review of maximum power point tracking algorithms for wind energy systems. *Renewable Sustainable Energy Rev.* **16**, 3220–3227 (2012).
10. C. Draxl, A. Clifton, B. M. Hodge, J. McCaa, The wind integration national dataset (wind) toolkit. *Appl. Energy* **151**, 355–366 (2015).
11. K. S. Hansen, R. J. Barthelmie, L. E. Jensen, A. Sommer, The impact of turbulence intensity and atmospheric stability on power deficits due to wind turbine wakes at Horns Rev wind farm. *Wind Energy* **15**, 183–196 (2012).
12. R. J. Stevens, C. Meneveau, Flow structure and turbulence in wind farms. *Annu. Rev. Fluid Mech.* **49**, 311–339 (2017).
13. R. J. Barthelmie *et al.*, Modelling and measuring flow and wind turbine wakes in large wind farms offshore. *Wind Energy* **12**, 431–444 (2009).
14. G. Marmidis, S. Lazarou, E. Pyrgioti, Optimal placement of wind turbines in a wind park using Monte Carlo simulation. *Renewable Energy* **33**, 1455–1460 (2008).
15. J. Meyers, C. Meneveau, Optimal turbine spacing in fully developed wind farm boundary layers. *Wind Energy* **15**, 305–317 (2012).
16. R. J. Stevens, D. F. Gayme, C. Meneveau, Effects of turbine spacing on the power output of extended wind-farms. *Wind Energy* **19**, 359–370 (2016).
17. General Electric, "GE announces Haliade-X, the world's most powerful offshore wind turbine" (2018). https://www.ge.com/renewableenergy/wind-energy/offshore-wind/haliade-x-offshore-turbine. Accessed 15 December 2018.
18. R. J. Stevens, B. F. Hobbs, A. Ramos, C. Meneveau, Combining economic and fluid dynamic models to determine the optimal spacing in very large wind farms. *Wind Energy* **20**, 465–477 (2017).
19. M. Gaumond *et al.*, "Benchmarking of wind turbine wake models in large offshore windfarms" in *The Science of Making Torque from Wind 2012: 4th Scientific Conference*, E. Seidel, D. Heinemann, M. Kühn, J. Peinke, S. Barth (IOP Publishing, Bristol, UK, 2012), vol. 555.
20. M. Z. Jacobson, M. A. Delucchi, A path to sustainable energy by 2030. *Sci. Am.* **301**, 58–65 (2009).
21. J. Lundquist, K. DuVivier, D. Kaffine, J. Tomaszewski, Costs and consequences of wind turbine wake effects arising from uncoordinated wind energy development. *Nat. Energy* **4**, 26–34 (2019).
22. J. Berg *et al.*, "Scaled wind farm technology facility overview" in *32nd ASME Wind Energy Symposium* (ASME, New York, NY, 2014), p. 1088.
23. P. Milan, M. Wächter, J. Peinke, Turbulent character of wind energy. *Phys. Rev. Lett.* **110**, 138701 (2013).
24. T. Das, V. Krishnan, J. D. McCalley, Assessing the benefits and economics of bulk energy storage technologies in the power grid. *Appl. Energy* **139**, 104–118 (2015).
25. G. C. Larsen, H. A. Madsen, K. Thomsen, T. J. Larsen, Wake meandering: A pragmatic approach. *Wind Energy* **11**, 377–395 (2008).
26. D. Nock, V. Krishnan, J. D. McCalley, Dispatching intermittent wind resources for ancillary services via wind control and its impact on power system economics. *Renewable Energy* **71**, 396–400 (2014).
27. J. R. Marden, S. D. Ruben, L. Y. Pao, A model-free approach to wind farm control using game theoretic methods. *IEEE Trans. Control Syst. Technol.* **21**, 1207–1214 (2013).
28. J. Annoni, P. M. Gebraad, A. K. Scholbrock, P. A. Fleming, J. W. v. Wingerden, Analysis of axial-induction-based wind plant control using an engineering and a high-order wind plant model. *Wind Energy* **19**, 1135–1150 (2016).
29. S. Boersma *et al.*, "A tutorial on control-oriented modeling and control of wind farms" in *2017 American Control Conference (ACC)* (IEEE, Piscataway, NJ, 2017), pp. 1–18.
30. P. Fleming *et al.*, Field-test results using a nacelle-mounted lidar for improving wind turbine power capture by reducing yaw misalignment. *J. Phys. Conf. Ser.* **524**, 012002 (2014).
31. Á. Jiménez, A. Crespo, E. Migoya, Application of a LES technique to characterize the wake deflection of a wind turbine in yaw. *Wind Energy* **13**, 559–572 (2010).
32. M. Adaramola, P. Å. Krogstad, Experimental investigation of wake effects on wind turbine performance. *Renewable Energy* **36**, 2078–2086 (2011).
33. F. Mühle *et al.*, Blind test comparison on the wake behind a yawed wind turbine. *Wind Energy Sci.* **3.2**, 883–903 (2018).
34. P. A. Fleming, A. Ning, P. M. Gebraad, K. Dykes, Wind plant system engineering through optimization of layout and yaw control. *Wind Energy* **19**, 329–344 (2016).
35. P. Gebraad, J. J. Thomas, A. Ning, P. Fleming, K. Dykes, Maximization of the annual energy production of wind power plants by optimization of layout and yaw-based wake control. *Wind Energy* **20**, 97–107 (2017).
36. P. Fleming *et al.*, A simulation study demonstrating the importance of large-scale trailing vortices in wake steering. *Wind Energy Sci.* **3**, 243–255 (2018).
37. C. L. Archer, A. Vasel-Be-Hagh, Wake steering via yaw control in multi-turbine wind farms: Recommendations based on large-eddy simulation. *Sustainable Energy Technol. Assess.* **33**, 34–43 (2019).
38. P. Fleming *et al.*, Initial results from a field campaign of wake steering applied at a commercial wind farm: Part 1. *Wind Energ. Sci.* **4**, 273–285 (2019).
39. P. Fleming *et al.*, Field test of wake steering at an offshore wind farm. *Wind Energy Sci.* **2**, 229–239 (2017).
40. J. Annoni *et al.*, "Efficient optimization of large wind farms for real-time control" in *2018 Annual American Control Conference (ACC)* (IEEE, Piscataway, NJ, 2018), pp. 6200–6205.
41. C. R. Shapiro, D. F. Gayme, C. Meneveau, Modelling yawed wind turbine wakes: A lifting line approach. *J. Fluid Mech.* **841**, R1 (2018).
42. M. F. Howland, J. Bossuyt, L. A. Martínez-Tossas, J. Meyers, C. Meneveau, Wake structure in actuator disk models of wind turbines in yaw under uniform inflow conditions. *J. Renewable Sustainable Energy* **8**, 043301 (2016).
43. M. F. Howland, A. S. Ghate, S. K. Lele, Influence of the horizontal component of Earth's rotation on wind turbine wakes. *J. Phys. Conf. Ser.* **1037**, 072003 (2018).
44. P. Gebraad *et al.*, Wind plant power optimization through yaw control using a parametric model for wake effects—a CFD simulation study. *Wind Energy* **19**, 95–114 (2016).
45. D. P. Kingma, J. Ba, Adam: A method for stochastic optimization. arXiv:1412.6980 (30 January 2017).
46. A. Niayifar, F. Porté-Agel, Analytical modeling of wind farms: A new approach for power prediction. *Energies* **9**, 741 (2016).
47. R. J. Stevens, D. F. Gayme, C. Meneveau, Coupled wake boundary layer model of wind-farms. *J. Renewable Sustainable Energy* **7**, 023115 (2015).
48. T. J. Larsen, H. A. Madsen, G. C. Larsen, K. S. Hansen, Validation of the dynamic wake meander model for loads and power production in the Egmond aan Zee wind farm. *Wind Energy* **16**, 605–624 (2013).
49. R. Damiani *et al.*, Assessment of wind turbine component loads under yaw-offset conditions. *Wind Energy Sci.* **3**, 173–189 (2018).
50. D. Medici, "Experimental studies of wind turbine wakes: Power optimisation and meandering," PhD thesis, (KTH Royal Institute of Technology, Stockholm, Sweden) (2005).
51. P. Fleming *et al.*, Simulation comparison of wake mitigation control strategies for a two-turbine case. *Wind Energy* **18**, 2135–2143 (2015).
52. W. Miao, C. Li, J. Yang, X. Xie, Numerical investigation of the yawed wake and its effects on the downstream wind turbine. *J. Renewable Sustainable Energy* **8**, 033303 (2016).
53. F. Campagnolo, V. Petrović, C. L. Bottasso, A. Croce, "Wind tunnel testing of wake control strategies" in *2016 American Control Conference (ACC)* (IEEE, Piscataway, NJ, 2016), pp. 513–518.
54. L. A. Martínez-Tossas, J. Annoni, P. A. Fleming, M. J. Churchfield, The aerodynamics of the curled wake: A simplified model in view of flow control. *Wind Energy Sci.* **4**, 127–138 (2019).
55. P. Fleming *et al.*, Investigation into the shape of a wake of a yawed full-scale turbine. *J. Phys. Conf. Ser.* **1037**, 032010 (2018).
56. K. A. Kragh, M. H. Hansen, Load alleviation of wind turbines by yaw misalignment. *Wind Energy* **17**, 971–982 (2014).
57. J. White, B. Ennis, T. G. Herges, "Estimation of rotor loads due to wake steering" in *2018 Wind Energy Symposium* (AIAA, Reston, VA, 2018), p. 1730.
58. N. Troldborg *et al.*, Numerical simulations of wake interaction between two wind turbines at various inflow conditions. *Wind Energy* **14**, 859–876 (2011).
59. J. Jonkman, *NWTC Design Codes (Fast)* (NREL, Boulder, CO, 2010).

PNAS
www.pnas.org

Supplementary Information for

Wind farm power optimization through wake steering

Michael F. Howland, Sanjiva K. Lele, and John O. Dabiri

To whom correspondence should be addressed: John O. Dabiri
E-mail: jodabiri@stanford.edu

This PDF file includes:

www.pnas.org/cgi/doi/10.1073/pnas.1903680116

Materials and Methods

Field experiment measurements. The wind inflow conditions are prescribed by the SCADA nacelle-mounted measurements of wind speed and nacelle direction. Wind speed is measured using both cup and sonic anemometers. The historical data wind rose for the most upwind turbine is shown in Fig. S1(a). The nacelle direction is controlled through a yaw control algorithm based upon the minimization between the wind turbine nacelle direction and a nacelle-mounted wind vane direction. The wind direction impinging upon the six turbines is specified by the nacelle direction of the most upstream turbine. The results are similar if the wind direction is prescribed by most downstream turbine which is not misaligned in the experiment. The wind speed is specified through an average of nearby uncontrolled baseline turbines since the wind speed measurement on a yawed turbine differs from the historical baseline data due to a change in the turbine axial induction. This change in axial induction alters the wind speed measurement on the yawed turbines. The mean absolute difference between the wind speed measured on the most upstream turbine nacelle and neighboring uncontrolled turbines increases by a factor of two when the most upstream turbine is yawed compared to the historical measurements. The Pearson-type correlation coefficient between the wind speeds measured by the most upstream turbine in the present study and the nearby turbines in the wind farm is above 0.9 in the historical measurements.

According to the historical measurements from the wind farm site, low-moderate wind speed occurs from the northwest approximately 10% of the time. Time steps during which wind turbines are curtailed, undergoing maintenance, or otherwise not collecting reliable power data when the velocity is above the cut-in are removed; these techniques are common in the processing of SCADA data (1). Instances when the most upstream turbine is below the cut-in power production are also removed since the wind direction measurements are unreliable below the cut-in speed. The SCADA data contained 546 and 664 one-minute averaged data samples for the low and moderate wind speeds for $330^\circ \pm 5^\circ$ inflow, respectively. The wind directions measured by the six optimized wind turbines during the experimental campaign are shown in Fig. S1(b). There are 17 and 22 one-minute averaged data samples for nocturnal $330^\circ \pm 5^\circ$ inflow at $5-6$ and $7-8$ m s^{-1} respectively from the experimental campaign. The details of the dataset can be seen in Table 1. Inflow from 330° and 335° at $6-7$ m s^{-1} exhibited power production gain over the baseline but was not included due to discrepancies among the wind speeds measured at neighboring turbines. The wind farm land is flat with no nearby complex terrain elements.

The experimental campaign also tested the model for the wind turbine power loss as a function of its yawing action. While actuator disk theory predicts a power loss of $\hat{P} = P\cos^3(\gamma)$ (2) where $\hat{P}$ is the yawed power state and P is the baseline power state, experiments have shown that $\hat{P} = P\cos^2(\gamma)$ may be more appropriate (3, 4). A comparison of the various models applied to the manufacturer provided wind turbine power curve with the data from the experimental yaw misalignment campaign is shown in Fig. S2.

Wake model. In previous studies, low-order model equations are typically discretized and solved pointwise in a domain with turbine power computed using numerical quadrature (5, 6). Due to spatial domain discretization, even low-order models previously used require too much computational effort to facilitate real-time active control (7, 8) due to numerical function evaluations at all grid points. The state space of yaw control is large and continuous. If we assume a yaw control system is only accurate to one degree and the yawing is constrained between $-30^\circ < \gamma < 30^\circ$ then each turbine has 60 possible states. The number of states for a wind farm with N_t turbines is then 60^{N_t}. For a six turbine wind farm, the state space has $4.7 \cdot 10^{10}$ discrete combinations. As a result, this problem requires efficient power computation and an efficient yaw optimization solver. Therefore, in the present study, we develop the analytic equations for power at each turbine in an arbitrary wind farm as a function of the yawing decisions of the upstream turbines.

With the recent discovery that wind turbines in yaw misalignment generate large-scale counter-rotating vortices much like an airfoil in a high angle of attack (9), a model based upon aerodynamic lifting line theory was developed (10, 11). The wake momentum deficit region is modeled as a velocity deficit spread along a Gaussian kernel (5, 12). Therefore, the streamwise velocity in the wake of a single turbine, i, is

$$u(x,y') = u_\infty - \delta u_i(x)\frac{D^2}{8\sigma_{0,i}^2}\exp\left(-\frac{(y'-y_{c,i}(x))^2}{2\sigma_{0,i}^2 d_{w,i}^2(x)}\right), \quad [1]$$

where streamwise and lateral directions are x and y respectively. The lateral direction in the frame of the upstream turbine is y'. The streamwise direction x is measured with respect to the upstream turbine i. The wake momentum deficit region, $\delta u(x)$, is assumed to be a Gaussian function (5) distributed along the laterally deflected centerline, y_c. The proportionality constant of the Gaussian wake is σ_0 and the normalized diameter of the wake is a function of the downstream distance x and is given by $d_w(x)$. The diameter of the wake is parameterized by k_w, the wake spreading coefficient. The vertical dimension is neglected in this model since the three dimensional modeling of the curled wake trailing a yaw misaligned turbine is the subject of on-going research (13) and the two dimensional model provides a lower bound on wake deflection (9, 14). The streamwise velocity deficit due to turbine i was computed by Shapiro *et al.* (11) from the linearized, stationary momentum equations with negligible viscosity and a parameterized turbulent viscosity and is given by

$$\delta u_i(x) = \frac{\delta u_{0,i}}{d_{w,i}^2(x)}\frac{1}{2}\left[1+\mathrm{erf}\left(\frac{x}{\sqrt{2}D/2}\right)\right]. \quad [2]$$

Since the streamwise coordinate x is measured with respect to the upstream turbine, $x \geq 0$. The initial streamwise velocity deficit $\delta u_{0,i}$ is prescribed by inviscid actuator disk theory (2), $\delta u_{0,i} = 2a_i u_\infty$. The axial induction factor is $a_i = 1/2\left(1-\sqrt{1-C_{T,i}\cos^2(\gamma_i)}\right)$ where the turbine thrust as a function of yaw is assumed to follow actuator disk theory (11). The nondimensional turbine thrust is given by $C_{T,i}$ and is provided by the turbine manufacturer.

In order to generalize Eq. 1 to an arbitrary number of upwind turbines, a wake superposition method must be selected. The wake may be superposed linearly (15) or according to a deficit of kinetic energy (16, 17). The deficit of kinetic energy method is the so-called sum-of-squares

wake superposition method

$$u(x,y) = u_\infty - \sqrt{\sum_i^{N_f} \Delta u_i^2}, \quad [3]$$

where $\Delta u_i = u_\infty - u_i(x,y)$ and N_f is the number of upwind turbines. When used with the Gaussian wake profile, the peak velocity deficit, occurring at the centerline, is superposed.

Some previous studies have used linear velocity deficit superposition rather than kinetic energy deficit (16). The following model focuses on linear wake superposition although it is straightforward to extend to sum-of-squares superposition. This method is concisely

$$u(x,y) = u_\infty - \sum_i^{N_f} \Delta u_i. \quad [4]$$

In order to compute power, the velocity must be averaged over the turbine rotor diameter. Using linear superposition, the area averaged effective velocity at an arbitrary turbine, j, in the wind farm is computed as

$$u_{e,j} = \frac{1}{A_j}\int_{A_j} u_j(x,y)dA = \frac{1}{A_j}\int_{A_j} (u_\infty - \Delta u_j)dA. \quad [5]$$

The surface area integration is, in general, perpendicular to the streamwise coordinate, in y and z. In the present two dimensional model, the integration is strictly in y. Using the momentum conserving superposition results in the effective velocity computed as

$$u_{e,j}(x) = u_\infty - \frac{1}{A_j}\int_{A_j} \sum_i^{N_f} \frac{\delta u_i(x) D^2}{8\sigma_{0,i}^2} \exp\left(-\frac{(y' - y_{c,i})^2}{2\sigma_i^2}\right) dA, \quad [6]$$

where $\sigma_i = \sigma_{0,i} d_{w,i}$. The upwind turbines are found automatically through knowledge of $d_{w,i}(x)$ and the turbine diameter and nacelle centroids. Further, since $\delta u_i \neq f(y)$, the effective velocity can be simplified to

$$u_{e,j}(x) = u_\infty - \sum_i^{N_f} \frac{\delta u_i(x) D^2}{8\sigma_{0,i}^2 A_j} \int_{A_j} \exp\left(-\frac{(y' - y_{c,i})^2}{2\sigma_i^2}\right) dA \quad [7]$$

which significantly simplifies the gradient computational graph. Following the analytic integration of Eq. 7, the effective area averaged velocity becomes

$$u_{e,j}(x) = u_\infty - \sum_i^{N_f} \frac{\sqrt{2\pi}\delta u_i(x) d_{w,i}(x) D}{16\sigma_{0,i}} \left[\text{erf}\left(\frac{y_T + D/2 - y_{c,i}(x)}{\sqrt{2}\sigma_{0,i} d_{w,i}(x)}\right) - \text{erf}\left(\frac{y_T - D/2 - y_{c,i}(x)}{\sqrt{2}\sigma_{0,i} d_{w,i}(x)}\right)\right]. \quad [8]$$

The downstream turbine lateral center is y_T.

The wake centerline $y_{c,i}$ for turbine i is computed as

$$y_{c,i} = \int_{x_{0,i}}^{x} \frac{-\delta v_i(x')}{u_\infty} dx', \quad [9]$$

where $x_{0,i}$ is the location of the upstream turbine. The lateral velocity, $\delta v(x)$, is computed similarly to Eq. 2

$$\delta v_i(x) = \frac{\delta v_{0,i}}{d_{w,i}^2(x)} \frac{1}{2}\left[1 + \text{erf}\left(\frac{x}{\sqrt{2}D/2}\right)\right]. \quad [10]$$

The normalized wake diameter is a function of x and is computed as

$$d_{w,i}(x) = 1 + k_{w,i} \log\left(1 + \exp[2(x/D - 1)]\right) \quad [11]$$

where $k_{w,i}$ is the wake spreading coefficient. Due to the invocation of Prandtl's lifting line model over an elliptical surface (11), the initial lateral velocity disturbance is uniform across the turbine's rotor area and is given analytically as

$$\delta v_{0,i} = \frac{1}{4} C_{T,i} u_\infty \cos^2(\gamma_i) \sin(\gamma_i). \quad [12]$$

Following (3), the coefficient of power then may be computed as

$$C_{P,i} = 4\eta a_{p,i}(1 - a_{p,i})^2 \cos^p(\gamma_i), \quad [13]$$

where $a_{p,i} = \frac{1}{2}\left(1 - \sqrt{1 - C_{T,i}}\right)$ and η is a tuning parameter used to match the manufacturer provided baseline C_P look-up table. From actuator disk theory, $p = 3$ (2), but recent large eddy simulations have shown $p = 1.88$ (18) for the NREL 5 MW wind turbine model. In the present study, we use $p = 2$, a more conservative estimate than that of (18). This is a fit which bears reasonable agreement to the experimentally observed trend of C_P with respect to γ for a variety of wind turbines (4). The power is then computed as

$$P_i = \frac{1}{2}\rho A_i C_p(a_{p,i}, \gamma_i) u_{e,i}^3. \quad [14]$$

Model calibration with historical data. In order to utilize the present wake modeling framework to predict optimal yaw angles, the model parameters k_w and σ_0 must be computed based on historical data. The model parameters are computed to reduce the power prediction error for the baseline, unyawed case of the wind farm. Wind turbine SCADA data of nacelle direction and wind speed are used as model inputs. Power SCADA data is used to calculate the error for a given state computation of the model using mean absolute error: $\text{MAE} = \frac{1}{m}\sum_{i=1}^{m}\left|\hat{P}_i - P_i\right|$ where P_i is the model predicted power for turbine i and $\hat{P}_i$ is the SCADA turbine power. The number of samples is given by m. The MAE is minimized using analytic gradient descent and therefore, the analytic gradients are derived.

With the MAE error function, the gradient with respect to the predicted power is

$$\frac{\partial \text{MAE}}{\partial P_j} = \text{sign}(\hat{P}_j - P_j), \tag{15}$$

where j is the index of the turbine downstream of turbine i. Importantly, the derivative of MAE is taken only with respect to the downstream turbine j to ensure that the correct direction of gradient descent is chosen. The derivative of the global farm MAE is not used since this will result in a single descent update direction (positive or negative) for all turbines in the wind farm. The derivative of the turbine specific MAE values are then averaged over the number of historical examples. The derivative of predicted power with respect to $u_{e,j}$ is

$$\frac{\partial P_j}{\partial u_{e,j}} = \frac{3}{2}\rho A_j C_{P,j} u_{e,j}^2. \tag{16}$$

If the wake is superposed using the sum-of-squares method, then

$$\frac{\partial u_{e,j}}{\partial c} = \frac{\partial u_{e,j}}{\partial \Delta u}\frac{\partial \Delta u}{\partial c}, \tag{17}$$

where c is a quantity of interest to be optimized. Therefore,

$$\frac{\partial u_{e,j}}{\partial c} = -\left(\sum_k^{N_f} \Delta u_k^2\right)^{-1/2} \Delta u_j \frac{\partial \Delta u_j}{\partial c}. \tag{18}$$

If superposition of linear velocity deficits (19) is used rather than sum-of-squares then

$$\frac{\partial u_{e,j}}{\partial c} = -\frac{\partial \Delta u_j}{\partial c}. \tag{19}$$

The velocity deficit Δu_j is a function of $d_{w,i}$, σ_i, and $\sigma_{0,i}$. Taking the gradient of Δu_j with respect to these three quantities gives

$$\frac{\partial \Delta u_j}{\partial d_{w,i}} = -\frac{\sqrt{2\pi}a_i D u_\infty}{8 d_{w,i}^2(x)\sigma_{0,i}}\left(1+\text{erf}\left(\frac{x'}{\sqrt{2}D/2}\right)\right)\left[\text{erf}\left(\frac{y_2'-y_{c,i}}{\sqrt{2\sigma_i^2(x)}}\right)-\text{erf}\left(\frac{y_1'-y_{c,i}}{\sqrt{2\sigma_i^2(x)}}\right)\right], \tag{20}$$

$$\frac{\partial \Delta u_j}{\partial \sigma_{0,i}} = -\frac{\sqrt{2\pi}a_i D u_\infty}{8 d_{w,i}(x)\sigma_{0,i}^2}\left(1+\text{erf}\left(\frac{x'}{\sqrt{2}D/2}\right)\right)\left[\text{erf}\left(\frac{y_2'-y_{c,i}}{\sqrt{2\sigma_i^2(x)}}\right)-\text{erf}\left(\frac{y_1'-y_{c,i}}{\sqrt{2\sigma_i^2(x)}}\right)\right], \tag{21}$$

and

$$\frac{\partial \Delta u_j}{\partial \sigma_i} = \frac{\sqrt{2\pi}a_i D u_\infty}{16 d_{w,i}^2(x)\sigma_{0,i}^2}\left[1+\text{erf}\left(\frac{x'}{\sqrt{2}D/2}\right)\right]\left(\left[\text{erf}\left(\frac{y_2'-y_{c,i}}{\sqrt{2\sigma_i^2(x)}}\right)-\text{erf}\left(\frac{y_1'-y_{c,i}}{\sqrt{2\sigma_i^2(x)}}\right)\right] + \frac{\sqrt{2/\pi}}{\sigma_i(x)}\left((y_1'-y_{c,i})e^{-(y_1'-y_{c,i})^2/2\sigma_i^2(x)} - (y_2'-y_{c,i})e^{-(y_2'-y_{c,i})^2/2\sigma_i^2(x)}\right)\right). \tag{22}$$

The two lateral extents of the turbine are given by $y_1' = y_T - D/2$ and $y_2' = y_T + D/2$ and x' is in the local frame of the upstream coordinate.

Finally, the gradient of σ_i with respect to $\sigma_{0,i}$ and $k_{w,i}$ are $\partial\sigma_i/\partial\sigma_{0,i} = d_{w,i}$ and $\partial\sigma_i/\partial k_{w,i} = \sigma_{0,i}\log\left(1+\exp[2(x/D-1)]\right)$. The gradient of $d_{w,i}$ with respect to $k_{w,i}$ is

$$\partial d_{w,i}/\partial k_{w,i} = \log\left(1+\exp[2(x/D-1)]\right) \tag{23}$$

The gradient of error at turbine j with respect to $\sigma_{0,i}$ of turbine i is therefore

$$\frac{\partial MAE_j}{\partial \sigma_{0,i}} = \frac{\partial MAE_j}{\partial P_j}\frac{\partial P_j}{\partial u_{e,j}}\left[\frac{\partial u_{e,j}}{\partial \sigma_i}\frac{\partial \sigma_i}{\partial \sigma_{0,i}} + \frac{\partial u_{e,j}}{\partial \sigma_{0,i}}\right] \tag{24}$$

and with respect to $k_{w,i}$ of turbine i is

$$\frac{\partial MAE_j}{\partial k_{w,i}} = \frac{\partial MAE_j}{\partial P_j}\frac{\partial P_j}{\partial u_{e,j}}\left[\frac{\partial u_{e,j}}{\partial \sigma_i}\frac{\partial \sigma_i}{\partial k_{w,i}} + \frac{\partial u_{e,j}}{\partial d_{w,i}}\frac{\partial d_{w,i}}{\partial k_{w,i}}\right] \tag{25}$$

Eqs. 24 and 25 are used to efficiently optimize the MAE using gradient descent.

The model coefficients for the model instance used in Fig. 2 are shown in Fig. S3. The coefficients for $u_\infty = 7\text{-}8$ m s^{-1} approximately asymptote after the second turbine which is consistent with previous studies (17) while the coefficients for $u_\infty = 5\text{-}6$ m s^{-1} do not because of the cut-in speed nonlinearity and dynamic wake meandering.

Gradient-based optimization. Gradient descent update can be stated concisely as

$$c^{t+1} = c^t - \alpha \frac{\partial f}{\partial c}, \tag{26}$$

where α is the learning rate (or step size), t is the optimization step, f is a function to be minimized, and again, c is an independent quantity of interest. For maximization, the subtraction becomes an addition. However, standard gradient ascent is particularly vulnerable to local extrema.

As a result, the Adam optimization method is used for the gradient update (20). Adam optimization is constructed based on the physical principle of momentum. The momentum term for an arbitrary function f and parameter c is $m^t = \beta_1 m^{t-1} + (1-\beta_1)\frac{\partial f}{\partial c}$ and the velocity term is $v^t = \beta_2 v^{t-1} + (1-\beta_2)(\frac{\partial f}{\partial c})^2$. The parameters β_1 and β_2 are set to the typical values of 0.9 and 0.999 (20). The model parameter is then updated as

$$c^{t+1} = c^t - \alpha \frac{m_t}{\sqrt{v_t}}, \tag{27}$$

Adam optimization is less sensitive to nonlinearities and saddle points in the objective function due to the hysteresis present in the gradient update.

Power optimization through yaw misalignment. The present optimization utilizes gradient ascent optimization in order to maximize the total power. The gradient ascent is performed using the Adam optimzer. In order to perform gradient optimization, the derivative of the total power function must be taken with respect to the optimization parameters. The gradients may be computed discretely. However, this method is prone to numerical errors and is more computationally expensive. Instead, we may borrow from recent literature in neural networks and computational graphs to compute the analytic derivative of P with respect to γ_i. The analytic derivative is based on the analytic form of the equation, and therefore, for the given system, is exact. We will derive the gradient update through successive application of the chain rule. First, we can take the derivative of the power with respect to the relevant parameters. The derivative of the total power with respect to the coefficient of power is

$$\frac{\partial P_i}{\partial C_{P,i}} = \frac{1}{2}\rho A_i u_{e,i}^3, \tag{28}$$

and with respect to the effective velocity is given by Eq. (16). Then, we can consider the equation for $C_{P,i}$,

$$\frac{\partial C_{P,i}}{\partial \gamma_i} = -8\eta a_{p,i}(1-a_{p,i})^2 \sin(\gamma_i)\cos(\gamma_i), \tag{29}$$

and

$$\frac{\partial C_{P,i}}{\partial a_{p,i}} = 4\eta(1 - 4a_{p,i} + 3a_{p,i}^2)\cos^2(\gamma_i). \tag{30}$$

We may further obtain

$$\frac{\partial a_{p,i}}{\partial C_{T,i}} = \frac{1}{4\sqrt{1-C_{T,i}}}. \tag{31}$$

These gradients are computed with respect to the current turbine of operation, i.e. the derivatives to this point are all derived with respect only the to yaw misaligned turbine itself. An example of this situation is a turbine in the last row of a wind farm. The turbines in the last row will always set $\gamma_i = 0$ to maximize power since the wake deflection which would result from their decision to yaw would not benefit any downwind turbines. This also manifests in the gradient ascent directly.

Computing the effective velocity at downwind turbines as a function of the yawing decisions of upwind turbines becomes more complex within a wind farm due to wake superposition. In particular, upstream turbine yawing decisions are not just based upon the maximization of their local $C_{P,i}$ but also must be based on the centerline of their wakes which affects the power generation at downstream turbines. Consider a turbine j whose wake impacts a turbine i. Since we are considering a Gaussian wake model in two dimensions, the effective velocity can be computed analytically by integrating the velocity $u_i(x,y)$ Eq. (1) over the turbine line, resulting in

$$u_{e,i} = \frac{u_\infty}{D_i}\left[D_i - \frac{\sqrt{2\pi}a_j D_i^2}{16 d_w(x)\sigma_0}\left(1+\text{erf}\left(\frac{x'}{\sqrt{2}D/2}\right)\right)\left[\text{erf}\left(\frac{y_2' - y_{c,j}}{\sqrt{2\sigma^2(x)}}\right) - \text{erf}\left(\frac{y_1' - y_{c,j}}{\sqrt{2\sigma^2(x)}}\right)\right]\right], \tag{32}$$

where y_1' and y_2' are the tips of the turbine which define the line integration in the frame of the upstream turbine. Then, the gradient of the effective velocity may be taken with respect to a_j and $y_{c,j}$. First,

$$\frac{\partial u_{e,i}}{\partial a_j} = -\frac{\sqrt{2\pi}u_\infty D_i}{16 d_w(x)\sigma_0}\left(1+\text{erf}\left(\frac{x'}{\sqrt{2}D/2}\right)\right)\left[\text{erf}\left(\frac{y_2' - y_{c,j}}{\sqrt{2\sigma^2(x)}}\right) - \text{erf}\left(\frac{y_1' - y_{c,j}}{\sqrt{2\sigma^2(x)}}\right)\right], \tag{33}$$

and

$$\frac{\partial u_{e,i}}{\partial y_{c,j}} = \frac{-u_\infty D_i a_j}{8 d_w^2(x)\sigma_0^2}\left(1+\text{erf}\left(\frac{x'}{\sqrt{2}D/2}\right)\right)\left[-\exp\left(-\frac{(y_2' - y_{c,j})^2}{2\sigma^2(x)}\right) + \exp\left(-\frac{(y_1' - y_{c,j})^2}{2\sigma^2(x)}\right)\right]. \tag{34}$$

These calculations can be done for each turbine upstream individually as a result of the linear wake superposition method.

The gradient axial induction factor a_j with respect to the yaw angle can be computed as

$$\frac{\partial a_j}{\partial \gamma_j} = \frac{-C_{T,j}\sin(\gamma_j)\cos(\gamma_j)}{2\sqrt{1 - C_{T,j}\cos^2(\gamma_j)}}. \quad [35]$$

The gradient of the centerline of the wake of the upstream wind turbine j with respect to γ_j must be computed. This gradient follows as

$$\frac{\partial y_{c,j}}{\partial \gamma_j} = \left[\cos^3(\gamma_j) - 2\sin^2(\gamma_j)\cos(\gamma_j)\right] \int_{x_{0,j}}^{x} \frac{-C_{T,j}}{8d_w^2(x')} \left[1 + \text{erf}\left(\frac{x'}{\sqrt{2}D/2}\right)\right] dx'. \quad [36]$$

The gradient of the centerline wake with respect to the upstream turbine's yaw angle requires numerical integration. Here, we use the second-order accurate trapezoidal numerical quadrature.

Finally, the total gradient of the power with respect to the yaw angle of a given turbine i is given as

$$\frac{\partial P_i}{\partial \gamma_i} = \frac{\partial P_i}{\partial C_{P,i}}\frac{\partial C_{P,i}}{\partial \gamma_i} + \frac{\partial P_i}{\partial C_{P,i}}\frac{\partial C_{P,i}}{\partial a_{p,i}}\frac{\partial a_{p,i}}{\partial C_{T,i}}\frac{\partial C_{T,i}}{\partial \gamma_i}. \quad [37]$$

The gradient of the power of a downstream turbine j with respect to the yawing decision of an upstream turbine i is

$$\frac{\partial P_j}{\partial \gamma_i} = \frac{\partial P_j}{\partial u_{e,i}}\frac{\partial u_{e,i}}{\partial y_{c,i}}\frac{\partial y_{c,i}}{\partial \gamma_i} + \frac{\partial P_j}{\partial u_{e,j}}\frac{\partial u_{e,j}}{\partial a_i}\frac{\partial a_i}{\partial \gamma_i}. \quad [38]$$

These gradients can be combined and the yaw angle may be updated according to Eq. (26) or Eq. (27).

Gradient Checking. The computed analytic gradient $\partial P/\partial \gamma$ is checked to ensure their accuracy since analytic gradients of complex computational graphs are prone to human error. This strategy is common in gradient-based machine learning approaches. Gradient checking involves comparing the analytic gradients to numerical gradients calculated with a finite differencing scheme and a small perturbation in the yaw angle. Second order accurate centered finite differencing is selected for the gradient calculation and the perturbation is $\epsilon = 10^{-8}$.

Here, we check the gradients for a model three turbine problem. The turbines are spaced evenly and $8D$ apart. The turbines are aligned in the lateral direction. The gradients are checked for the last turbine first since this gradient will only manifest at this turbine itself. The gradients are checked for $-45^\circ < \gamma < 45^\circ$. The gradient for the most downwind turbine is simple and agrees to machine precision with the numerical gradient. This is shown in Fig. S4(a). The gradient for the most upwind turbine is more complicated as a result of the spatial nonlinearity of the wake (21). Upstream turbine gradients with respect to yaw will manifest in the power of downstream turbines through the wake centroid y_c. The gradient for the most upwind turbine is shown in Fig. S4(b). The analytic gradient agrees well with the numerical gradient with small discrepancies at large yaw angles. The discrepancy at large yaw angles is likely due to sharp nonlinearities in the velocity profiles (6).

The gradients are also checked for the model parameters k_w and σ_0. These gradients are computed for the unyawed operating condition and are computed for the most upstream turbine in the example problem. The gradients are shown in Fig. S5 and show good agreement with the centered finite differencing scheme with $\epsilon = 10^{-8}$.

Northwest inflow optimization for Summerview Wind Farm. Following model calibration to historical baseline data, the model is optimized through yaw misalignment. Here, we focused on the yaw optimization of the six utility-scale turbines shown in Fig. 3 for inflow from the northwest, particularly 325°-335°. Angle inflow direction changes of 10° result in different wake conditions. At 325° the downstream turbines are in partial wakes of the upstream turbines while at 335° inflow the turbines are in the full wakes. Due to experimental limitations of the utility-scale turbines, the yaw misalignment angle could not be changed as a function of time during the experiment. As such, we aggregated the optimization results for the inflow between 325°-335° to select the optimal yaw angles. The experimental yaw angles were selected as angles which provided robust power increase for the range of inflow angles specified since field wind conditions are unknown *a priori*. This robustness also considered wind speed. Overall, the aggregated optimization resulted in $\gamma = 20^\circ$ clockwise for turbines one through five and $\gamma = 0^\circ$ for turbine six. Since the optimization is sensitive to wind speed and layout conditions, a control system which allows for dynamic yaw maneuvers could result in significantly improved wind farm performance. The dynamic model calibration and yaw optimization algorithm is summarized in Alg. 1. In general, the FieldObservation() algorithm would involve a state estimation technique such as the Kalman Filter. The power is observed through SCADA data. The wake parameters, k_w and σ_0, are updated according to the field observation using gradient descent. The yaw angles are optimized using ForwardProp() which calculates the state of the power generation and BackProp() which computes the analytic dervatives. The yaw angles are updated with Adam optimization.

In general, gradient-based optimization is subject to local maxima which may inhibit the search for globally optimal solutions. Recent work in deep neural networks suggest that in high dimensional space, true local extrema are uncommon but saddle points are frequent (22). To handle saddle points or potential local extrema, the present approach can be straightforwardly extended to include an optimization approach such as a genetic algorithm to be used in tandem with the analytic gradients. The present yaw optimization of the six utility-scale turbines was not sensitive to initialization for the inflow angles tested.

To illustrate the use of the present yaw optimization algorithm, we will consider inflow from 330° at $u_\infty = 7.5\ \text{m s}^{-1}$. The model calibration for this condition is given in Fig. 2(b). The learning rate is $\alpha = 10^{-4}$. The yaw angles are initialized to zero for all turbines. The convergence criteria is based on the total power generation. If

$$\frac{|P_{t+1} - P_t|}{|P_t|} < \epsilon \quad [39]$$

then the optimization has converged. The convergence criteria is $\epsilon = 10^{-8}$ in the present study. The optimization results can be seen in Fig. S6. This six turbine utility-scale optimization takes approximately 1 second on a standard laptop computer.

Algorithm 1 Maximize Power through Yaw Optimization

procedure MAXIMIZEPOWER($k_{w,0}$, $\sigma_{0,0}$, γ_0, α, β_1, β_2, ϵ)
  $P \leftarrow$ FieldObservation()
  $k_w,\ \sigma_0 \leftarrow$ UpdateWakeParams(P, $k_{w,0}$, $\sigma_{0,0}$, α, β_1, β_2, ϵ)
  $t = 0$, $m_0 = 0$, $v_0 = 0$
  while $|P_t - P_{t-1}| \,/\, |P_{t-1}| > \epsilon$ **do**
    $P_t \leftarrow$ ForwardProp(k_w, σ_0, γ)
    $\partial P/\partial\gamma \leftarrow$ BackProp(P_t, k_w, σ_0, γ)
    $m_t = \beta_1 m_{t-1} + (1-\beta_1)\partial P/\partial\gamma$
    $v_t = \beta_2 v_{t-1} + (1-\beta_2)(\partial P/\partial\gamma)^2$
    $\gamma = \gamma + \alpha(m_t/\sqrt{v_t})$
    $t \leftarrow t+1$
  return γ

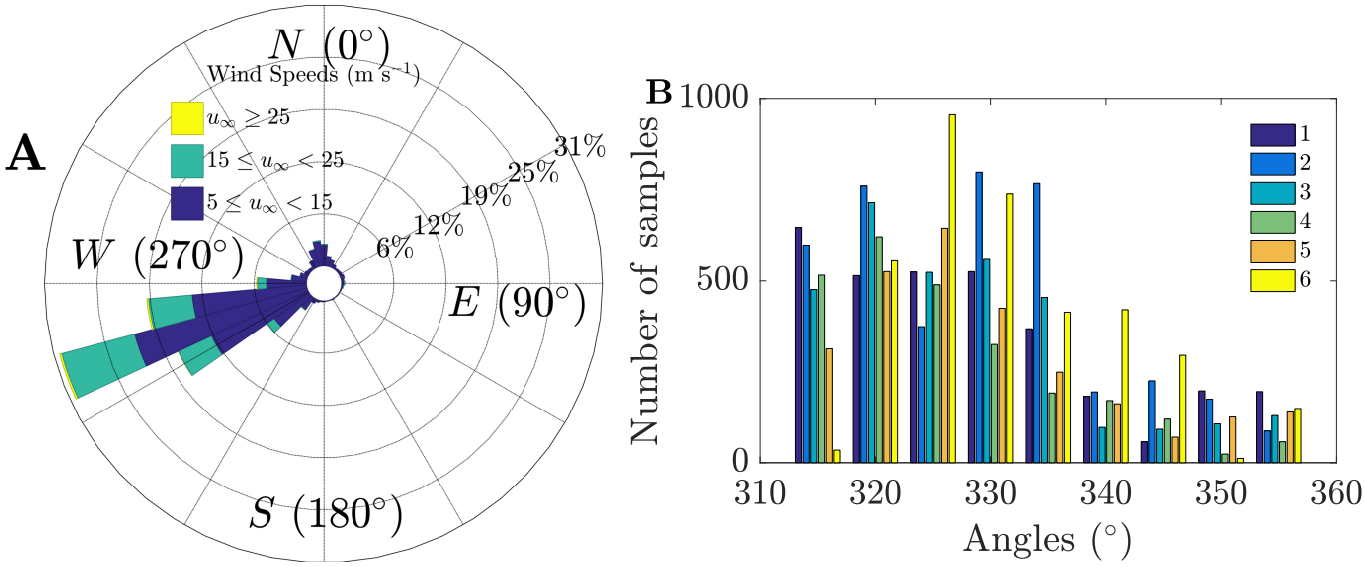

Fig. S1. (a) Wind rose for turbine one for the historical SCADA data. (b) Nacelle directions during the experimental yaw campaign for the six controlled turbines. The angles are given in bins of 10° width.

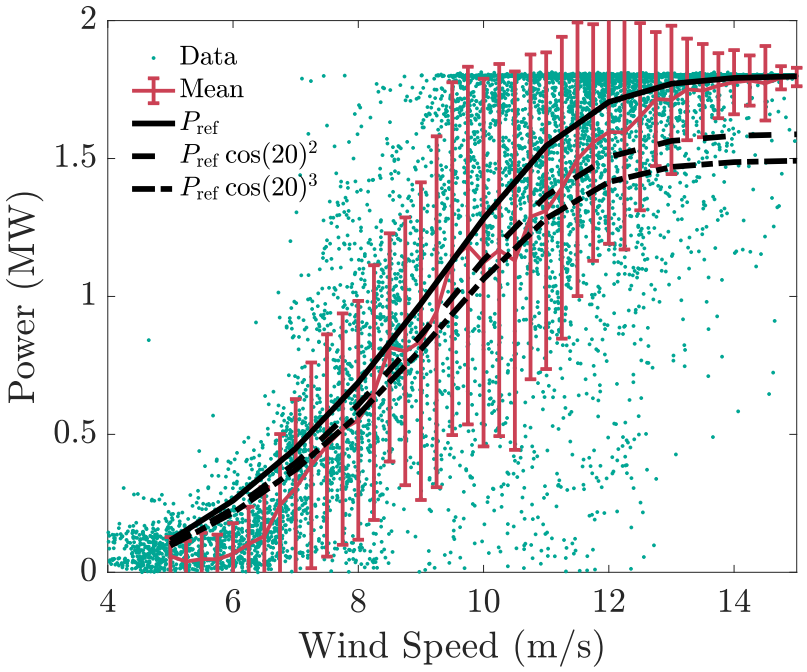

Fig. S2. Power curve for the yaw misalignment experiment for turbine one. The raw, uncurtailed one-minute averaged data is shown with dots. Averaged data in $0.25\ \mathrm{m\ s^{-1}}$ bins are shown in red. The errorbars represent one standard deviation in the data and are assumed to be symmetric about the mean. The manufacturer provided power curve is shown in solid black. The manufacturer provided power curve with models of $\cos^2(\gamma)$ and $\cos^3(\gamma)$ are shown with dashed and dashed-dotted curves respectively.

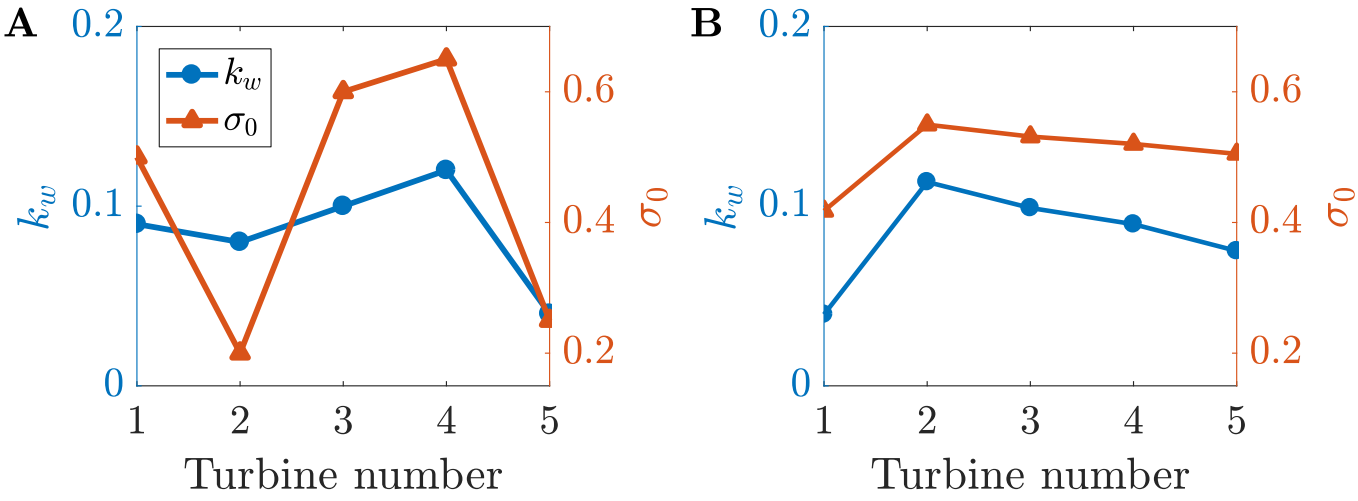

Fig. S3. The model coefficients k_w and σ_0 for the model calibration using historical SCADA data for (a) $u_\infty = 5\text{-}6\ \mathrm{m\ s^{-1}}$ and (b) $u_\infty = 7\text{-}8\ \mathrm{m\ s^{-1}}$ with $330^\circ \pm 5^\circ$ inflow direction. The model produces turbine power predictions shown in Fig. 2.

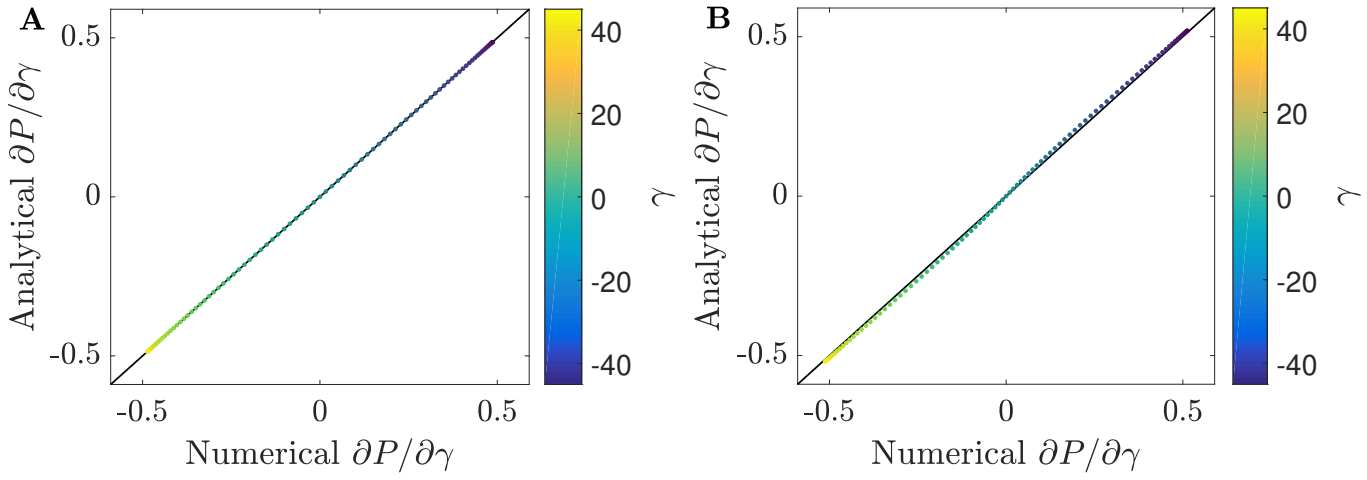

Fig. S4. Gradient checking for the analytic gradients of modeled power with respect to the yaw angle. The analytic gradients are plotted as a function of the numerical gradients. A line of unity slope is given by the black line. The gradients are checked for $-45^\circ < \gamma < 45^\circ$. The gradients are computed in an example three turbine model problem for (a) the most downstream turbine and (b) the most upstream turbine.

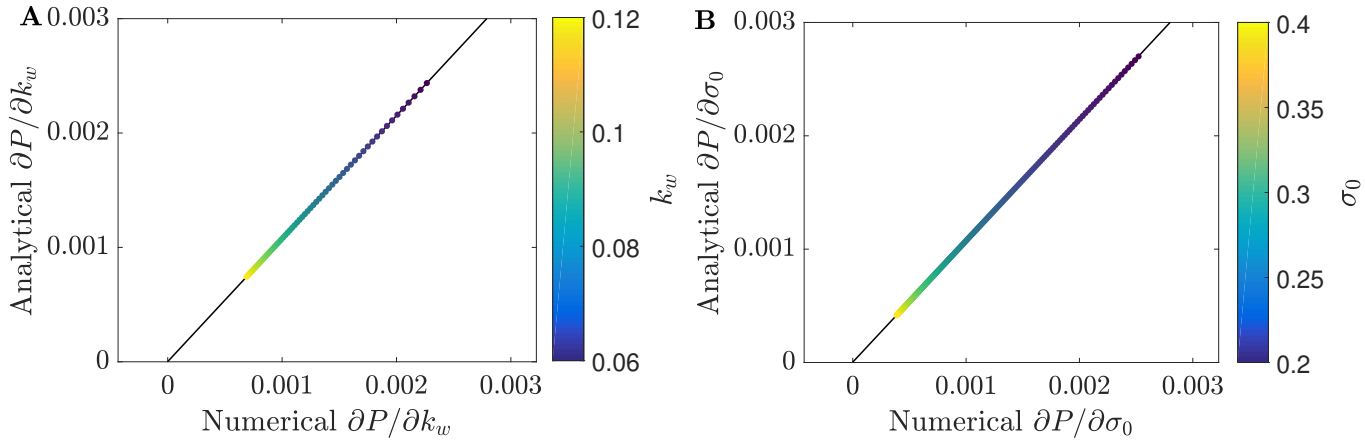

Fig. S5. Gradient checking for the analytic gradients of modeled power with respect to the model parameters (a) k_w and (b) σ_0. The analytic gradients are plotted as a function of the numerical gradients. A linear fit is given by the black line. The gradients are checked for various conditions of k_w and σ_0 and for the upstream turbine in the three turbine model problem.

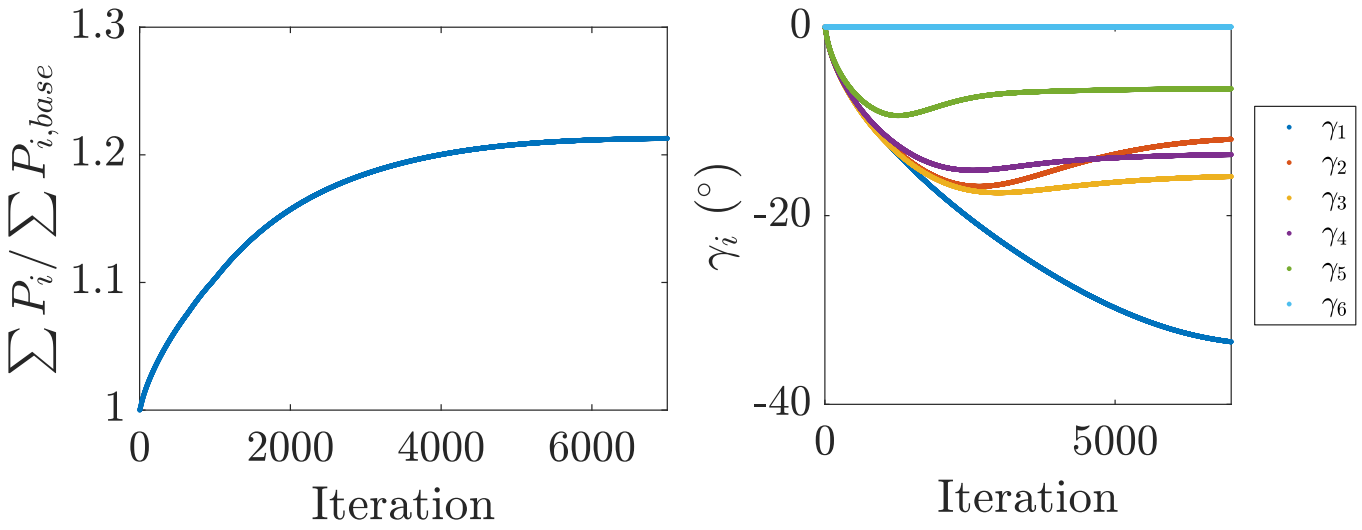

Fig. S6. Yaw optimization for the six utility-scale turbines for inflow from 330°. The inflow velocity is $u_\infty = 7.5\ \mathrm{m\ s^{-1}}$. The model calibration is given by Fig. 2(b).

References

1. Nygaard NG (2014) Wakes in very large wind farms and the effect of neighbouring wind farms in *Journal of Physics: Conference Series*. (IOP Publishing), Vol. 524, p. 012162.
2. Burton T, Jenkins N, Sharpe D, Bossanyi E (2011) *Wind Energy Handbook*. (John Wiley & Sons).
3. Gebraad P, et al. (2016) Wind plant power optimization through yaw control using a parametric model for wake effects—a CFD simulation study. *Wind Energy* 19(1):95–114.
4. Medici D (2005) Experimental studies of wind turbine wakes: power optimisation and meandering Ph.D. thesis (KTH Royal Institute of Technology).
5. Bastankhah M, Porté-Agel F (2014) A new analytical model for wind-turbine wakes. *Renewable Energy* 70:116–123.
6. Fleming PA, Ning A, Gebraad PM, Dykes K (2016) Wind plant system engineering through optimization of layout and yaw control. *Wind Energy* 19(2):329–344.
7. Boersma S, et al. (2017) A tutorial on control-oriented modeling and control of wind farms in *2017 American Control Conference (ACC)*. (IEEE).
8. Bay CJ, Annoni J, Taylor T, Pao L, Johnson K (2018) Active power control for wind farms using distributed model predictive control and nearest neighbor communication in *2018 Annual American Control Conference (ACC)*. (IEEE).
9. Howland MF, Bossuyt J, Martínez-Tossas LA, Meyers J, Meneveau C (2016) Wake structure in actuator disk models of wind turbines in yaw under uniform inflow conditions. *Journal of Renewable and Sustainable Energy* 8(4):043301.
10. Milne-Thomson LM (1973) *Theoretical Aerodynamics*. (Courier Corporation).
11. Shapiro CR, Gayme DF, Meneveau C (2018) Modelling yawed wind turbine wakes: a lifting line approach. *Journal of Fluid Mechanics* 841.
12. Bastankhah M, Porté-Agel F (2016) Experimental and theoretical study of wind turbine wakes in yawed conditions. *Journal of Fluid Mechanics* 806:506–541.
13. Martínez-Tossas LA, Annoni J, Fleming PA, Churchfield MJ (2019) The aerodynamics of the curled wake: a simplified model in view of flow control. *Wind Energy Science (Online)* 4(NREL/JA-5000-73451).
14. Fleming P, et al. (2018) A simulation study demonstrating the importance of large-scale trailing vortices in wake steering. *Wind Energy Science* 3(1):243–255.
15. Katic I, Højstrup J, Jensen NO (1987) A simple model for cluster efficiency in *European Wind Energy Association Conference and Exhibition*.
16. Vermeer L, Sørensen JN, Crespo A (2003) Wind turbine wake aerodynamics. *Progress in Aerospace Sciences* 39(6-7).
17. Stevens RJ, Gayme DF, Meneveau C (2015) Coupled wake boundary layer model of wind-farms. *Journal of Renewable and Sustainable Energy* 7(2):023115.
18. Annoni J, et al. (2018) Efficient optimization of large wind farms for real-time control in *2018 Annual American Control Conference (ACC)*. (IEEE).
19. Niayifar A, Porté-Agel F (2016) Analytical modeling of wind farms: A new approach for power prediction. *Energies* 9(9):741.
20. Kingma DP, Ba J (2014) Adam: A method for stochastic optimization. *arXiv preprint arXiv:1412.6980*.
21. Gebraad P, Thomas JJ, Ning A, Fleming P, Dykes K (2017) Maximization of the annual energy production of wind power plants by optimization of layout and yaw-based wake control. *Wind Energy* 20(1):97–107.
22. LeCun Y, Bengio Y, Hinton G (2015) Deep learning. *Nature* 521(7553):436.